

IMAGING SATURATION DURING FLOW IN FRACTURED CHALK: EMPHASIZING RECOVERY MECHANISMS, CAPILLARY CONTINUITY AND SCALING

Bjørn Gerry Viksund¹, Sverre Hetland¹, Arne Graue¹ and Bernard A. Baldwin²

¹ Department of Physics, University of Bergen, Norway

² Phillips Petroleum Company Research Center, Oklahoma, USA.

ABSTRACT

Nuclear tracer imaging was used to monitor in-situ local brine saturation and its change during spontaneous imbibition and waterflood experiments in chalk. Outcrop chalk was used both for uniformity and limited access to reservoir core. Imbibition rates were dependent on the amount of exposed surface and the length of the sample. The imbibition endpoint was uniform for all samples and independent of both the exposed surface and the length of the sample. Fractures under the current experimental conditions had no detectable effect on imbibition, indicating that good capillary contact had been achieved in these experiments. A scaling law proposed by Ma and Morrow brought the oil production rates from all the samples into a better fit.

INTRODUCTION

The oil production mechanism in fractured chalk reservoirs has long been believed to be governed by spontaneous imbibition from water filled fractures with the expelled oil being flushed through the fracture network to the production wells. Recently, however, it has been suggested that if there is sufficient capillary contact between the chalk matrices on either side of a fracture, the oil may also move through the matrix. If so, viscous displacement of oil could also play a role during waterfloods of fractured chalk reservoirs.

Discussions on the relative importance of viscous- versus capillary forces in oil recovery from fractured chalk reservoirs have resulted in experimental and simulation investigations of recovery mechanism(s), boundary conditions and applicability of scaling laws for predicting oil production from fractured chalk.

This study was initiated by a need to quantitatively assess the relative importance of viscous and spontaneous recovery mechanisms because a two-dimensional fractured chalk laboratory reservoir model is under construction for the experimental simulation of oil recovery. In this physical model the simultaneous competition between viscous, capillary and gravitational forces can be studied, because the changes of in-situ local saturations will be monitored with a nuclear tracer imaging technique (1,2). The experimental 2D-reservoir model will be composed of stacked matrix blocks with selected fracture geometries. Knowing the relative importance of viscous versus imbibition forces and the effect of capillary continuity across fractures is important for modeling oil production from fractured reservoirs.

EXPERIMENTAL

Application of the nuclear tracer imaging technique has been shown to provide an enhanced description of the water/oil displacement during laboratory flooding experiments (3,4). Information on one dimensional fluid saturation distributions was obtained by labelling the fluid phase(s) with nuclear tracer(s). In the two phase flow experiments performed in this work only one tracer was used, ²²Na in the form of NaCl dissolved in water. Radiation was detected by a moveable detector; the magnitude of the counts were proportional to the saturation of the labelled phase, water, and hence normalized to obtain the in-situ brine saturation. The saturation of the second phase, oil, was determined by difference. The nuclear tracer imaging technique used to obtain saturation data has been described in detail (1,2).

Effluent production was compared to in-situ saturation measurement to verify true saturation data. Correction for dead volume was taken into account for the effluent production profiles.

The core material was obtained from the Dania quarry at Ålborg, Denmark. Core data of the outcrop chalk is found in Table 1. Laboratory tests indicate favorable brine imbibition for samples from this outcrop. Compared to other outcrop chinks the Dania samples were less fragile and gave porosity, permeability, connate water saturation and imbibition properties which were similar to the North Sea chalk reservoirs.

The other materials used in this test were: NaCl obtained from Phil Inc. with a purity of 99.5%, CaCl₂ obtained from Phil Inc. with a purity of 99.5%, n-Decane obtained from Phil Inc. with a purity of higher than 95%, Lamp oil obtained from Statoil and Marcol 172 obtained from Esso. All materials were used as received. The physical properties of the fluids are summarized in Table 2.

To minimize potential absorption of ²²NaCl the cores were first flushed with nonradioactive NaCl brine before flooding with radioactive brine. Calcium chloride, CaCl₂, was added to the brine to minimize dissolution of the chalk. The physical properties of the brine are included in Table 2.

The core floods were conducted in standard biaxial core holders using a slight confinement pressure. Due to the fragile nature of the chalk material care was taken not to exceed 10 bar (147 psi) net confinement pressure.

A schematic drawing of the apparatus used for the water- and oil floods is shown in Figure 1. Spontaneous imbibition tests were done partly on epoxy coated cores and partly in core holders. The end pieces for cores used in imbibition tests were supplied with three ports. Water flowed in the lower port with a flow rate of 0.2 ml/min, flushed the face of the core with water to remove expelled oil droplets and forced the expelled oil out the upper ports. A schematic drawing of 1D-, 2D- and 3D imbibition tests are shown in Figure 2a and Figure 2b.

RESULTS AND DISCUSSIONS

Figure 3 shows a miscible displacement, where radioactive brine displaced non radioactive brine in a representative core, CHD-10, with a flow rate of .14 ml/min. These displacements were monitored to evaluate dispersion and ion-adsorption. The uniformity of the flood front during brine injection, a function of permeability, and the endpoint image, a function of porosity distribution, indicated that these cores contained no gross heterogeneities. If there had been permeability variations the injection would have produced fingers and if there had been porosity variations the final image would have shown a wide variation in intensity.

Figure 4 exhibits changes in brine saturation during brine imbibition from one end of core CHD-3, a 1D test. Local water saturations along the axis of the core, at various times, are plotted as a function of core length. The initial water saturation was uniform at 28%PV. Spontaneous brine imbibition from the left side of the core produced 37%PV of oil, giving an average Swf of 65%PV, or 51% recovery of OIP (Oil In Place). The saturation gradients are monotonic and generally parallel to each other corroborating the uniform nature of the core. In the 1D test the imbibition is counter current, i.e. the oil flows opposite of the direction of the imbibing water, because the exposed face must act as both the inlet and outlet.

Figure 5 shows the time development of the water saturation profiles for water imbibition from both ends of core CHD-3, a 2D test. Imbibition started at both ends and the profiles were roughly symmetric about the center of the core. This again corroborates the uniform nature of the core. The saturation gradients in Figure 5 are roughly the same as in the 1D case until there was significant water in the middle, >3.1hr. Swf was 67% and the recovery efficiency was 54% OIP. This configuration still produces counter current flow since water is flowing in and oil is flowing out of both faces. Even if oil produced by imbibition of water flowing in face 1 flows out face 2, i.e. it is cocurrent with water flow from face 1, it is still flowing counter current to water flowing in from face 2. Discussions on this subject have been reported (5,6).

Figure 6 compares the corresponding effluent profiles for the 1D and 2D cases. The oil production rates

from each end of the 2D core are comparable to the initial oil production rate of the 1D test, but the endpoints are reached sooner. However, the total production profile for the 2D test showed a faster production rate and slightly higher production compared to the 1D test, although, the latter may represent the experimental uncertainty. These results showed that the rate of oil production by spontaneous imbibition was significantly dependent on the surface area exposed to water.

Figure 6 also includes imbibition results from Core CHD-8, which was half the length of CHD-3. The 1D-imbibition of this core roughly corresponded to one half of the 2D-imbibition of CHD-3. This indicated a linear relationship for scaling of oil recovery with respect to core length. The longer imbibition time of the 1D imbibition of CHD-3 can be related to the longer distance the fluids must travel for water to expell oil, not just the available surface area.

Figure 7 shows the imbibition production profiles of 1D-, 2D- and 3D-imbibition for the cores CHD-3 and CHD-8. The amount of oil recovered by spontaneous imbibition was the same for all configurations. However, the imbibition production rate was much higher during the 3D-imbibition. In fact, the imbibition rate during 3D-imbibition was so fast that in-situ saturation profiles could not be recorded with reasonable accuracy, using the same radioactive brine as in the 1D test. The average distance the water and oil must move during the 3D imbibition will be much more complex than in the 1D and 2D cases since not only are both end exposed but the surface of the cylinder was also exposed.

In Figure 8 the results of a repeatability test for the 3D imbibition experiment is shown. The repeatability of the experiment was very good.

The extent of capillary contact between stacked cores was evaluated during low rate oilfloods by looking for capillary end effects between the individual cores in the composite cores and by measuring the local distribution and rate of the brine advancement during 1D spontaneous imbibition in the stacked core system.

Figure 9 shows a low rate oilflood, 0.1 ml/min, in a stacked core system, composed of cores CHD-8 and CHD-9. The data showed no evidence of end effects, capillary hold up of the wetting phase, at the fracture between the two cores, position 8.1 cm. However, at the end of the composite core system, at position 18 cm, the end effect is clearly visible in curves 0.31 through 0.61 PV. After oil break through, 0.35 PV of oil injected, the flood rate was increased to 0.5 ml/min, resulting in a saturation distribution shown in the figure when 0.61 PV had been injected. The flow rate was again increased, to 3.8 ml/min, and the resulting brine saturation distribution is represented by the profile taken when 3.09PV had been injected. The final Swi was reached after 10.4 PV of the more viscous Marcol 172 had been injected, giving a total of 13.5 PV of oil injected. The Marcol 172 was injected with a maximum flow rate of .25ml/min and the core flushed in both directions. The viscous oil then was flushed out by 10PV decane prior to the next experiment.

A 1D-imbibition experiment was performed on these stacked cores, see Figure 10, with water entering from the left side of the system. These profiles, taken at different times or amounts of oil recovered, exhibited a jump in saturation at the fracture at 8.1 cm. These results suggest that the low permeable, 5mD, core, CHD-9, had a significantly higher capillary pressure and literally sucked brine out of CHD-8. The higher saturation in CHD-9 at the imbibition endpoint corroborated this suggestion. These results also indicated a high degree of capillary continuity between the two cores. After 80 hours of imbibition an average Swf was reached at 79%PV, the average Swf in CHD-8 was approximately 74%PV and for CHD-9 approximately 82%PV. This corresponds to a 70% recovery efficiency of OIP. Relative permeability to water was measured to $k_{rw}=0.3$.

Another sequence of a low rate oilflood and a 1D-imbibition test was performed for a stacked core system consisting of three cores, core CHD-8, CHD-9 and CHD-10. The results are virtually identical to the plots in Figure 10 and are not shown here.

The conclusion that capillary contact was achieved was based on the lack of any observed local end effects

for the stacked cores under the low rate oilflood and also due to the fact that the 1D spontaneous imbibition continued through all of the three stacked cores, without any observable delay. This capillary contact may have been aided by an axial pressure applied when the end pieces of the core holder were hand-tightened. The pressure between the cores were estimated to be 0.9 bar (13 psi).

All imbibition experiments were followed by waterfloods and the recovery of the two processes compared. For the water wet systems, spontaneous imbibition was found to be as efficient as forced waterfloods, even with a significant differential pressure over the core (3). The final water saturations for this outcrop chalk appeared to be constant, except for the one low permeability core CHD-9. Consistent repeatability of properties is a significant advantage when using outcrop chalk versus real core.

To evaluate vertical capillary continuity, experiments were conducted when cores were stacked in a vertical configuration. Figure 11 shows the low rate oilflood performed downwards, right to left, in a vertically stacked core system consisting of cores CHD-1, CHD-2 and CHD-3*, labelled CHD-123. Each of these cores was 10.0 cm long. No capillary hold up was observed during the low rate oilflood; see the profile obtained when 0.23PV oil was injected. The later brine saturation distributions were obtained after the low viscosity oil was flushed out by a high viscosity oil, Marcol 172, and the flow rate steadily increased. The final water saturation distribution, after 8.6PV of oil had been injected, was obtained under a differential pressure of 30 bars.

The subsequent imbibition experiment was performed with the water entering at the bottom of the stacked core system. Imbibition as a function of time is shown in Figure 12 with the bottom of the composite core to the left. The water imbibed upwards, toward the right in Figure 12, through all of the three cores with no apparent holdup. The endpoint saturation, S_{wf} , was comparable to the corresponding endpoint water saturation for the horizontal imbibition experiments. In spite of the fact that the brine imbibed vertically there was no evidence of gravity segregation at the fractures between the individual cores. Figure 13 shows the effluent production for similar length horizontally and vertically stacked core systems. There appears to be no significant difference between oil production recovered by spontaneous brine imbibition in horizontally or vertically stacked core systems of limited heights.

Figure 14 shows the oil production from cores which have different lengths. The composite core systems appeared to be in capillary contact and thus simulate long cores. The cores of similar length, for example, CHD-3 and CHD-89, gave similar imbibition rate curves. Most of the cores imbibed to similar endpoints. It should be noted that the endpoint is in pore volume of oil recovered, not absolute amounts. Note that there appears to be a consistent trend for an increased induction period proportional to the core length.

Scaling laws are used to transform laboratory data on small core plugs into results which can be used in a mathematical simulator for predicting hydrocarbon movement and recovery in reservoirs. For imbibition in fractured rock a scaling law has been presented by Ma and Morrow (7,8 and references cited therein). In this scaling the imbibition time is converted to a dimensionless time factor, based on core and fluid properties, and typical imbibition characteristics for the given rock/fluid system. The proposed scaling law is a modified version of one suggested by Mattax and KYTE (9), based on work by Rapoport (10).

$$t_d = t \sqrt{\frac{k}{\Phi} \frac{\sigma}{\mu_{gm}} \frac{1}{L_c^2}}$$

where t_d is the dimensionless time, t imbibition time, k absolute permeability, Φ porosity, σ interfacial tension, μ_{gm} the geometric mean of the oil and water viscosities and L_c a characteristic length.

The modifications proposed by Ma and Morrow are the use of an average mean for the fluid viscosities, rather than only the oil viscosity, and a different characteristic length, L_c ,

$$L_c = \sqrt{\frac{V}{\sum_{i=1}^n \frac{A_i}{X_{Ai}}}}$$

where X_{Ai} is the distance travelled by the imbibition front from the exposed surface to the no-flow boundary (7). V is the bulk volume of the matrix and A_i the area open to imbibition at the i th direction.

Figure 15 shows the scaled imbibition characteristics for CHD-3 and CHD-8, with respect to different surface area exposed to water for imbibition. After scaling it was a significant better fit for the four imbibition curves compared to the original data in Figure 7. The results corroborate the validity of the scaling with respect to imbibition rate.

In Figure 16 the scaling has been applied to cores with various lengths and stacked core systems in capillary contact. Although, the individual imbibition curves do not fall on top of each other, as in Figure 15, there was a somewhat closer fit than for the original data, Figure 14. It appeared that the induction time increased with core length and that imbibition rate generally decreased with core length and the number of fractures. If the area in capillary contact between the stacked cores was a fraction of the butted end surface area, this could induce a delay or reduction in imbibition rates. This will again impact the average effective permeability for the stacked core system. It needs to be mentioned that for some of the cores, in particular CHD-9, the permeability was considerably different, and may contribute to poorer scaling, which was based on an average absolute permeability.

CONCLUSIONS

The nuclear tracer imaging system has been verified to be applicable for monitoring the local saturation development under spontaneous water imbibition and forced water injection in chalk.

Nuclear imaging of the fluid displacement gave reliable information on water frontal velocities, local saturation distribution, initial and final water saturation and impacts from heterogeneities.

Final oil production for 1D-, 2D- and 3D imbibition were similar for Dania outcrop chalk. Imbibition rate and oil production were dependent on exposed surface area and the length of the core.

Good repeatability of immobile water saturation profiles were obtained under similar experimental conditions, both the average saturation and the distribution of the reduced water saturation were reproduced.

Capillary continuity was obtained in stacked core systems, with a slight axial pressure applied, during the imbibition experiment.

A scaling law for oil production by spontaneous water imbibition was tested and found useful, but more data is needed for verification of its general applicability.

ACKNOWLEDGEMENTS

The authors acknowledge permission to publish the above paper from Phillips Petroleum Company Norway and Co-venturers, including Fina Exploration Norway S.C.A., Norsk Agip A/S, Elf Petroleum Norge A/S, Norsk Hydro Produksjon a.s., Total Norge A/S, Den norske stats oljeselskap a.s., Elf Rex Norge A/S and Saga Petroleum a.s.

REFERENCES

1. Lien, J.R., Graue, A., Kolltveit, K.: "A Nuclear Imaging Technique for Studying Multiphase Flow in a Porous Medium at Oil Reservoir Conditions", Nucl. Instr. & Meth., A271 (693,700) 1988.
2. Graue, A., Kolltveit, K., Lien, J.R., Skauge, A.: "Imaging Fluid Saturation Development in Long Coreflood Displacements", SPE# 21101, Proc. SPE 1990 Latin American Petroleum Conference, Rio de Janeiro, Brazil, Oct. 14-19, 1990.
Published in: SPEFE, Vol.5, No.4, (406-412), Dec. 1990.
3. Graue, A.: "Nuclear Tracer Saturation Imaging of Fluid Displacement in Low-Permeability Chalk", Proc.: SPE Rocky Mountain Regional/Low Permeability Reservoirs Symposium, Denver, CO, USA, April 26-28, 1993.
4. Graue, A.: "Imaging the Effects of Capillary Heterogeneities on Local Saturation Development in Long-Core Floods", SPE# 21101, Proc. SPE 1990 Latin American Petroleum Conference, Rio de Janeiro, Brazil, Oct. 14-19, 1990.
Published in: SPEDC, March 1994.
5. Bourbiaux, B., Kalaydjian, F.: "Experimental Study of Cocurrent and Countercurrent Flows in Natural Porous Media", Proc.: SPE Annual Technical Conference and Exhibition, Houston, TX, Oct. 2-5, 1988.
6. Cuiiec, L.E., Bourbiaux, B., Kalaydjian, F.: "Imbibition in Low-Permeability Porous Media: Understanding and Improvement of Oil Recovery", Proc.: SPE/DOE 7th Symp. on Enhanced Oil Recovery, Tulsa, OK, April 22-25, 1990.
7. Ma, S., Morrow, N.R.: "Influence of Fluid Viscosity on Mass Transfer between Fractures and Matrix", paper CIM 95-94, Petr. Soc. of CIM Ann, Tech. Meeting, Banff, Alberta, Canada, May 14-17, 1995.
8. Zhang, X., Morrow, N.R., Ma, S.: "Experimental Verification of a Modified Scaling Group for Spontaneous Imbibition", Proc.: SPE Annual Tech. Conf. and Exhibition, Dallas, TX, Oct. 22-25, 1995.
9. Mattax, C.C., Kyte, J.R.: "Imbibition Oil Recovery from Fractured, Water Drive Reservoirs", SPEJ (June 1962) 177-88.
10. Rapoport, L.A.: "Scaling Laws for Use in Design and Operation of Water-Oil Flow Models", Trans AIME, Vol.204, 143-50, 1955.

Table 1. Core data

Core#	Outcrop	Porosity [%]	Abs.Perm. [mD]	Pore Vol. [cc]	Length [cm]	Diam. [cm]
CHD-1	Dania	37.	28.	74.3	10.0	5.0
CHD-2	Dania	36.	19.	73.4	10.0	5.1
CHD-3 ¹	Dania	37.	26.	74.0	10.0	5.1
CHD-123	Dania	36.	24. ²	221.7	30.0	5.1
CHD-8	Dania	38.	45.	57.1	8.1	4.8
CHD-9	Dania	33.	5.	63.4	10.2	4.8
CHD-10	Dania	41.	27.	90.6	11.1	5.0
CHD-89	Dania	37.	8. ²	120.5	18.3	5.0
CHD-8910	Dania	39.	11. ²	211.1	29.4	5.0
CHD-3	Dania	42.	3.	127.5	16.1	4.9

¹ CHD-3* is a different core than CHD-3

² Permeability is calculated based on the measured absolute permeability for each core

Table 2. Fluid data

Fluid	Density [g/cm ³]	Viscosity cp@20°C	Composition
Brine	1.05	1.09	5wt% NaCl + 5wt% CaCl ₂
Lamp oil	.74	1.43	n-parafins: C9-C13
Marcol 172	.85	72.	White Mineral Oil
n-decane	.73	.92	Purity > 95%

TABLE 3. Experimental schedule and saturation history of outcrop cores

Flood data	CHD-3		CHD-123	CHD-8			CHD-89	CHD-8910
<u>Miscible flood:</u>								
Flow rate: q [ml/min]	.15		.09				.15	
<u>Oilflood#:</u>	1	2		1	2	3		
Flow rate: q [cc/min]	0.1-4.	0.1-4.	0.1-10.	0.5-4.	0.5-4.	0.5-4.	0.1-3.8	.3-4.8
Oil viscosity [cp]	1.43;72.	1.43;72.	0.92;72.	72.	72.	72.	1.43-72.	1.43
Sw _i [%PV]	28.	29.	23.	27.	26.	31.	31.	30.
Endpoint kr _o	0.9	1.0	1.0	.7	.7	.8	.8	.7
<u>Imbibition#:</u>	1	2		1	2	3		
Boundary condition	1D	2D	1D	3D	1D	3D	1D	1D
Oil viscosity [cp]	.92	.92	.92	.92	.92	.92	.92	.92
dSw [%PV]	37.	38.	37.	43.	42.	39.	48.	37.
Sw _f [%PV]	65.	67.	60.	70.	68.	70.	79.	67.
R _f [%OIP]	51.	54.	48.	59.	57.	57.	70.	53.
<u>Waterflood#:</u>	1	2		1	2	3		
Flow rate: q [cc/min]	.27	.23	.15	.74	.74	.74	.34	.62
Oil viscosity [cp]	.92	.92	.92	.92	.92	.92	.92	.92
dSw [%PV]	0.	0.	9.	0.	0.	0.	2.	3.
Sw _f [%PV]	65.	67.	69.	70.	68.	70.	81.	70.
R _f [%OIP]	51.	54.	60.	59.	57.	57.	72.	57.
Endpoint kr _w	.4	.4	.1	.3	.3	.4	.3	.3

kr_w - relative permeability to waterkr_o - relative permeability to oilR_f - recovery efficiencySw_i - initial water saturation

dSw - produced fluid

Sw_f - final water saturation

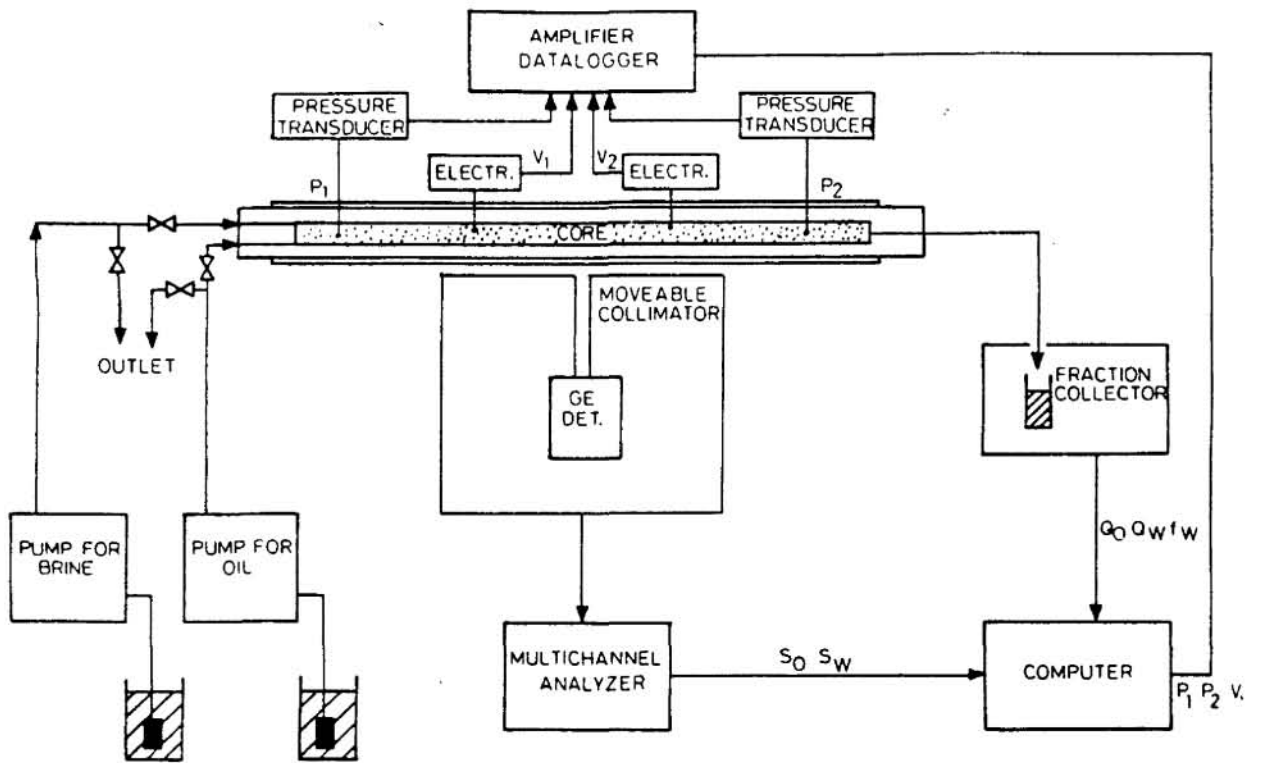


Figure 1. Schematic drawing of the Flow-rig utilizing the nuclear tracer imaging technique.

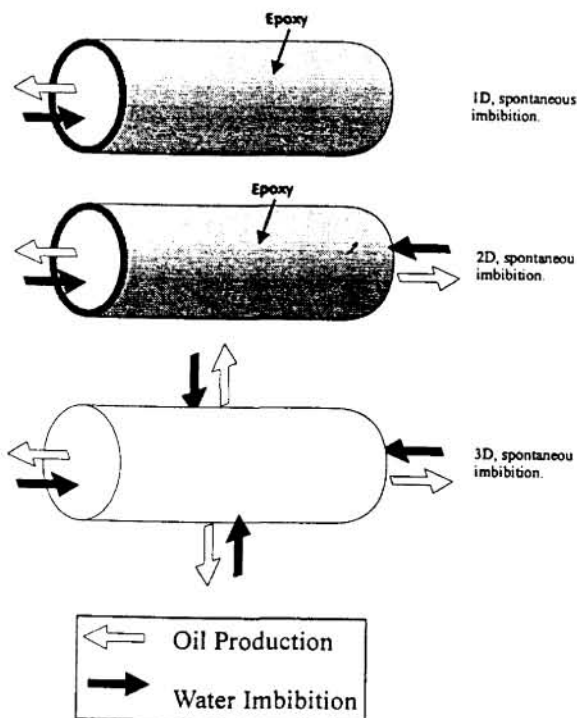


Figure 2a. Visualization of the notation 1D, 2D and 3D imbibition in core plugs.

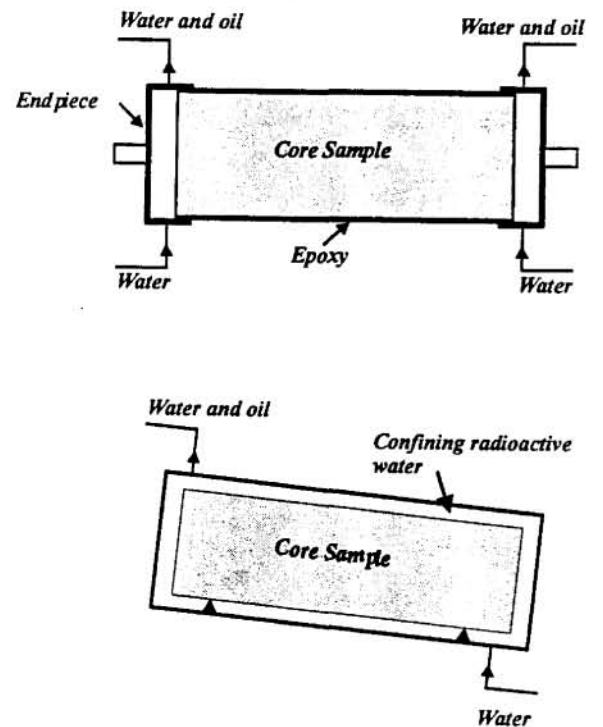


Figure 2b. 1D and 2D imbibition setup of epoxy coated cores (upper), 3D imbibition setup in lucide cylinder (lower).

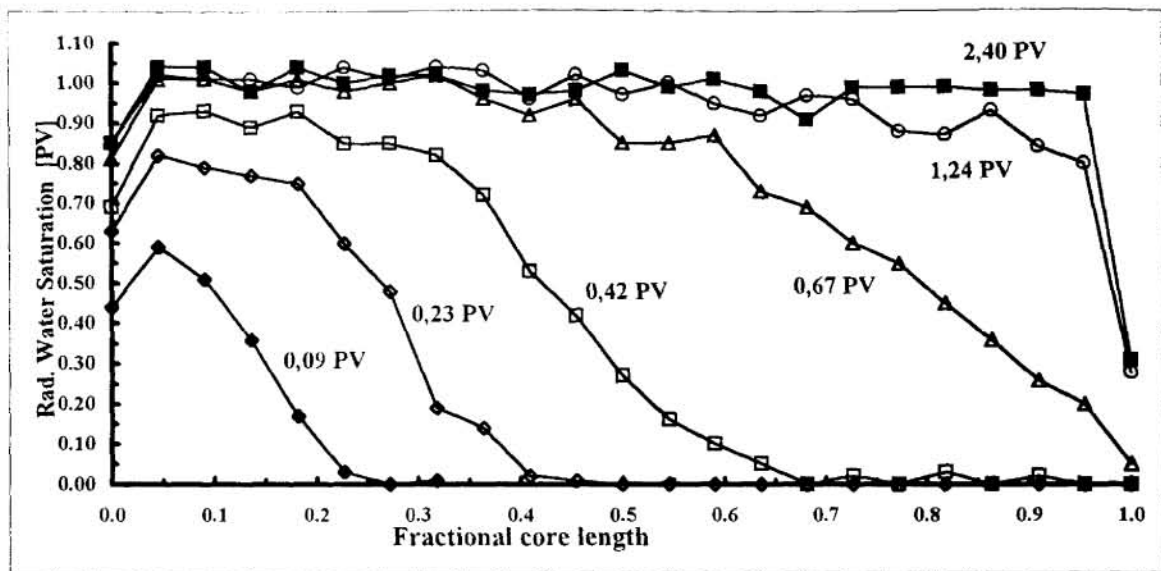


Figure 3. Miscible brine/brine displacement for CHD-10.

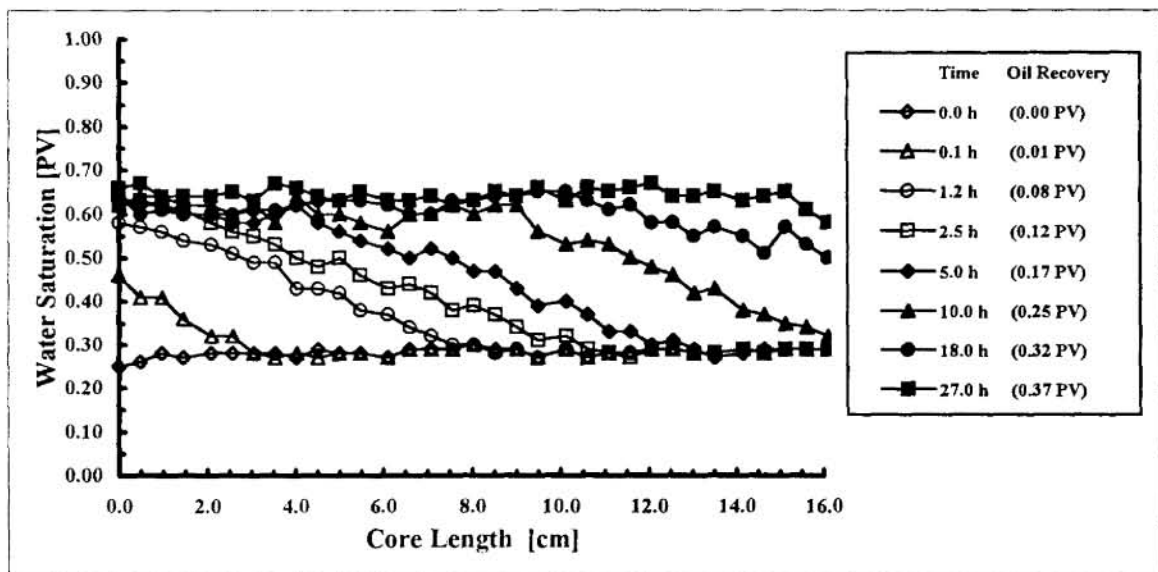


Figure 4. 1D imbibition in CHD-3.

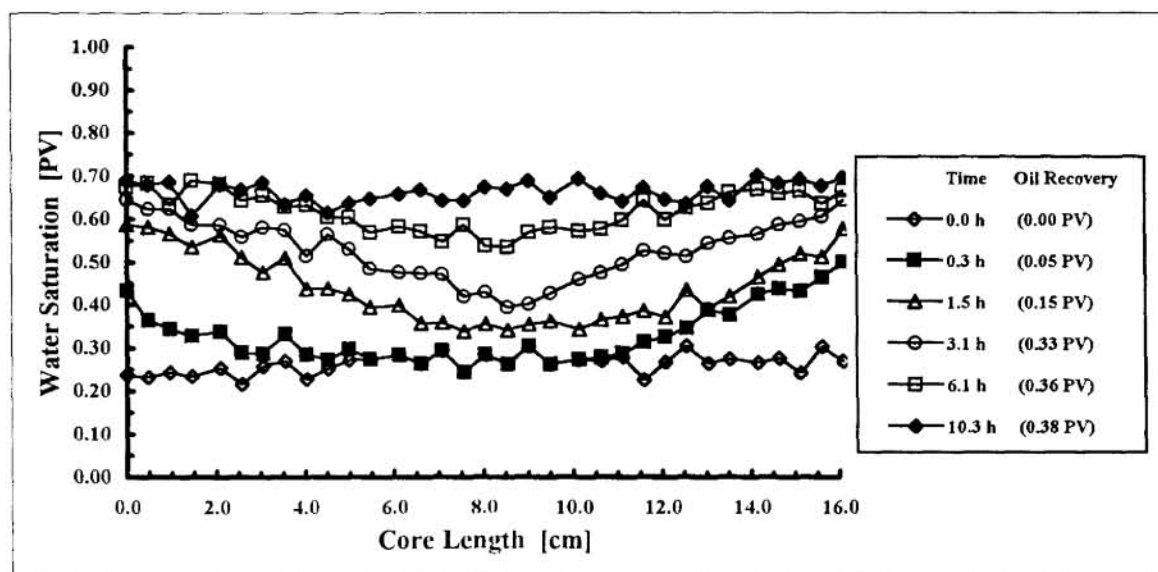


Figure 5. 2D imbibition in CHD-3.

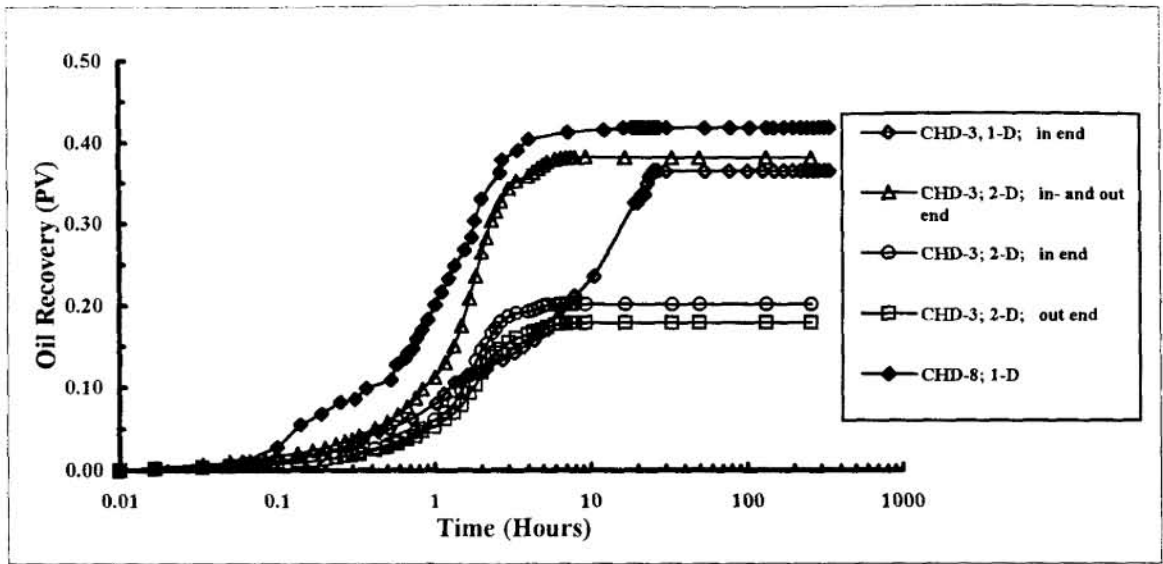


Figure 6. Oil production from 1D and 2D spontaneous imbibition in CHD-3 (16.1 cm) and 1D spontaneous imbibition in CHD-8 (8.1 cm).

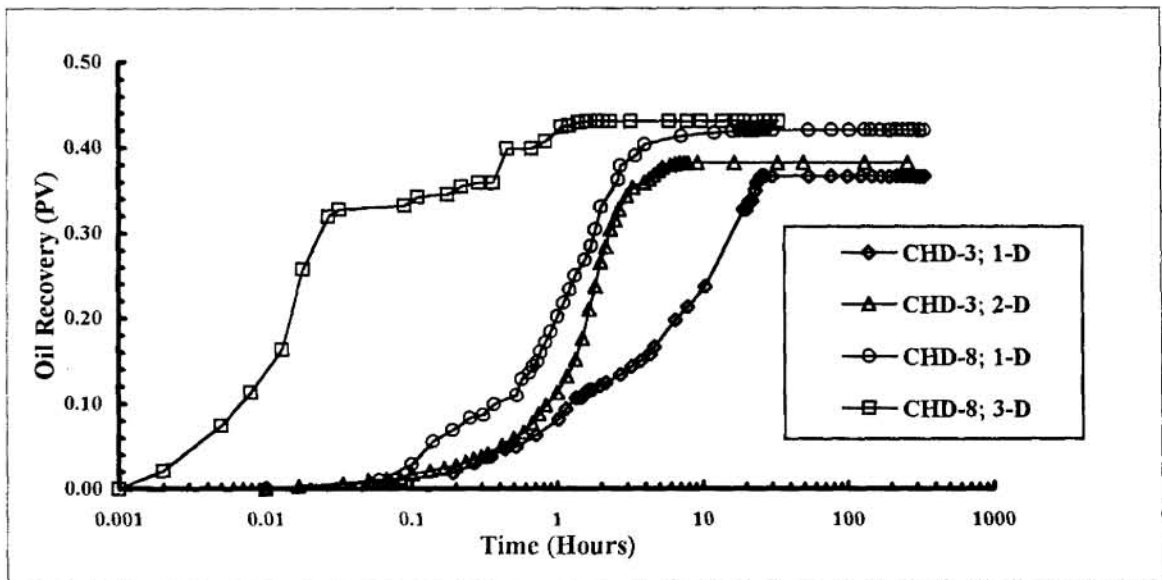


Figure 7. Different surface area of chalk exposed to water in 1D, 2D and 3D imbibition of CHD-3 (16.2 cm) and CHD-8 (8.1 cm).

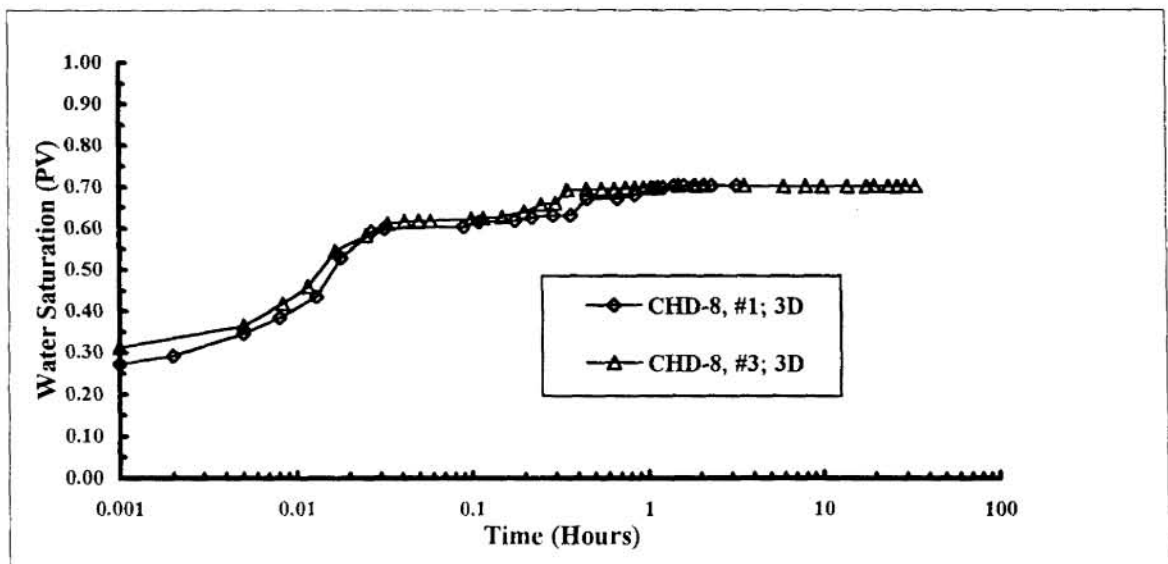


Figure 8. Reproducibility of 3D spontaneous imbibition in CHD-8.

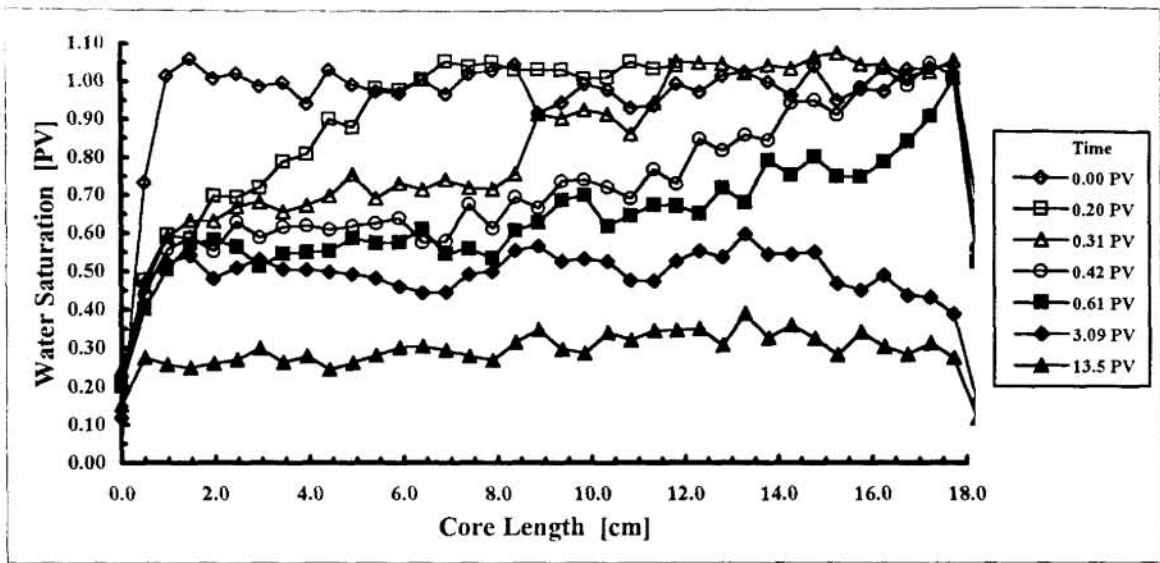


Figure 9. First oilflood of the horizontally stacked cores CHD-89 (CHD-8: 8.1 cm, CHD-9: 10.2 cm).

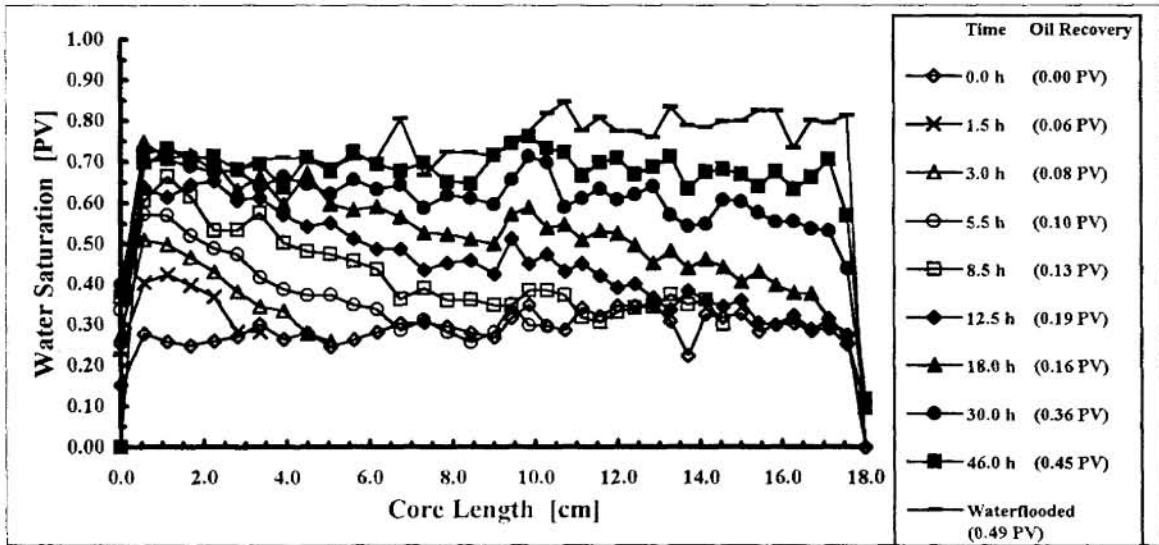


Figure 10. 1D imbibition in the horizontally stacked cores CHD-89 (CHD-8: 8.1 cm, CHD-9: 10.2 cm).

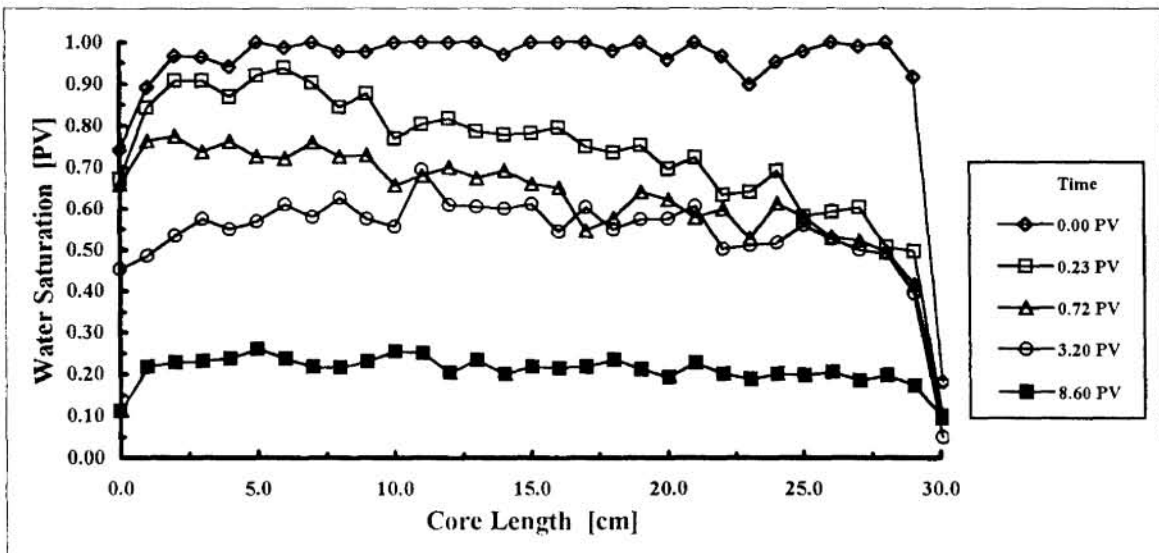


Figure 11. First oilflood of the vertically stacked cores CHD-123 (CHD-1: 10.0 cm, CHD-2: 10.0 cm, CHD-3*: 10.0 cm).

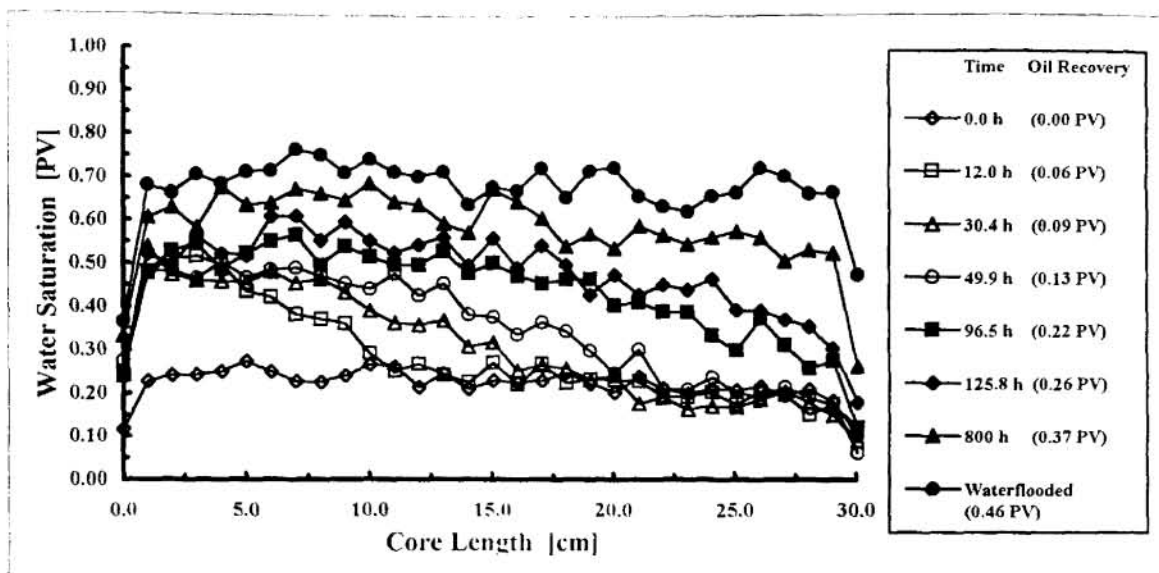


Figure 12. 1D spontaneous imbibition in the vertically stacked cores CHD-123 (CHD-1: 10.0 cm, CHD-2: 10.0 cm, CHD-3*: 10.0 cm).

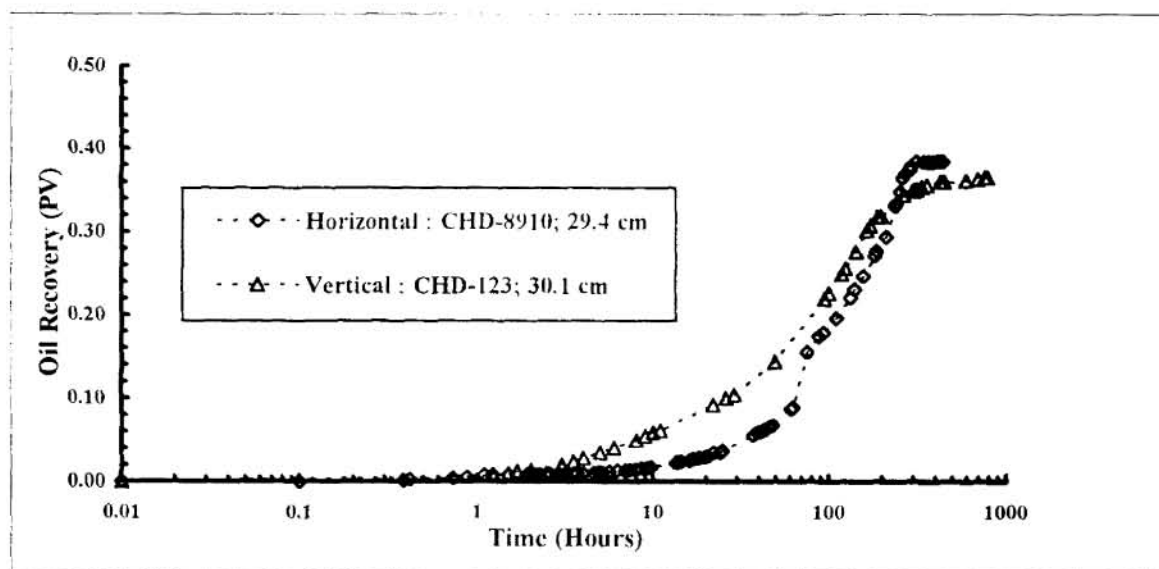


Figure 13. Vertical and horizontal 1D spontaneous imbibition for fractured chalk.

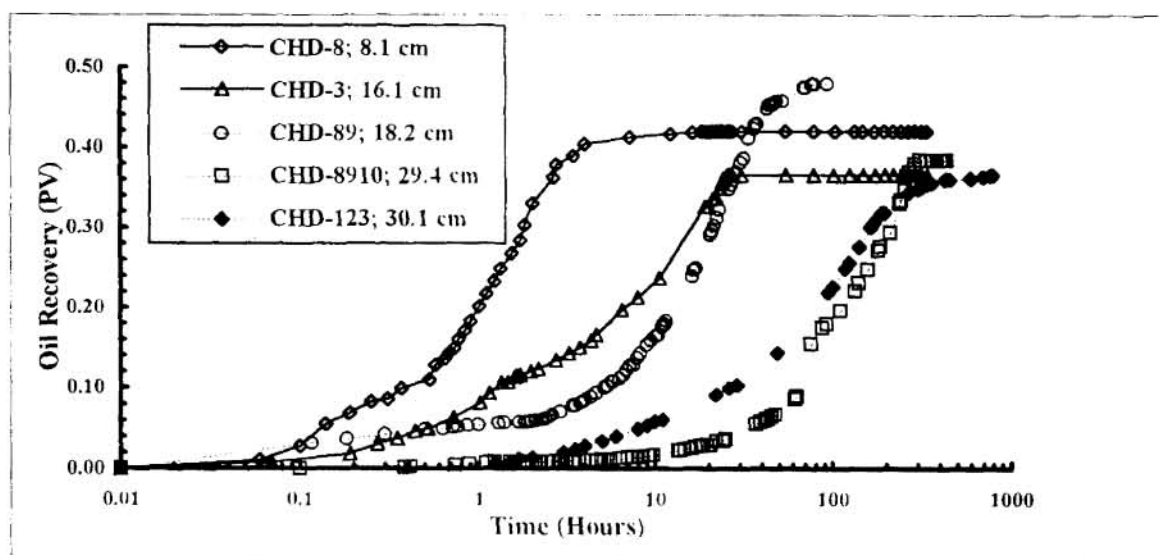


Figure 14. 1D spontaneous imbibition; different core lengths, fractured and unfractured chalk.

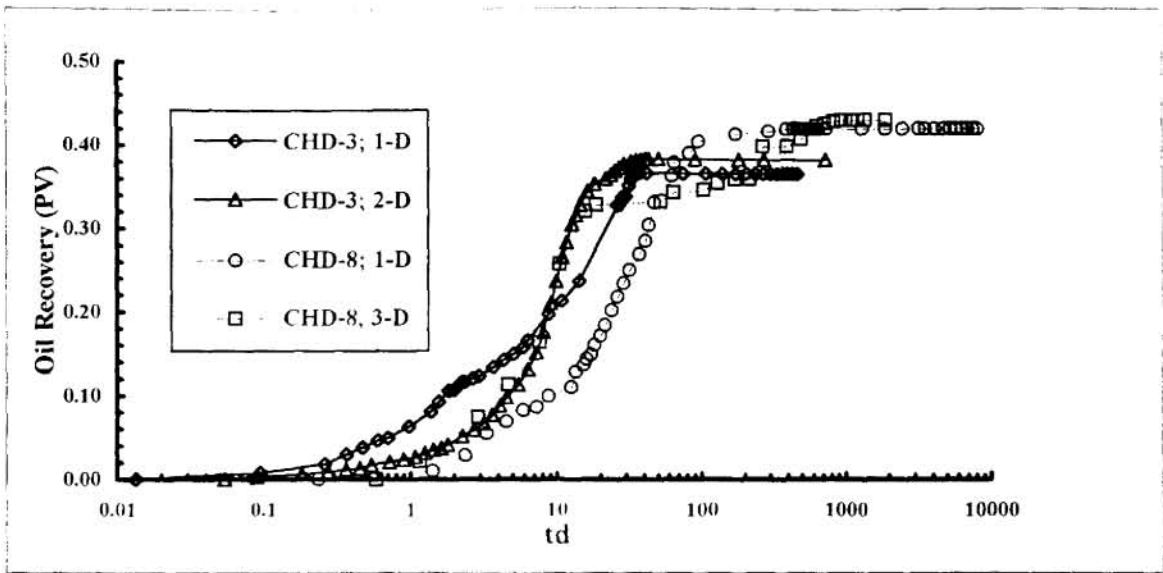


Figure 15. Scaled spontaneous imbibition, cores with different areas exposed to brine; unfractured cores.

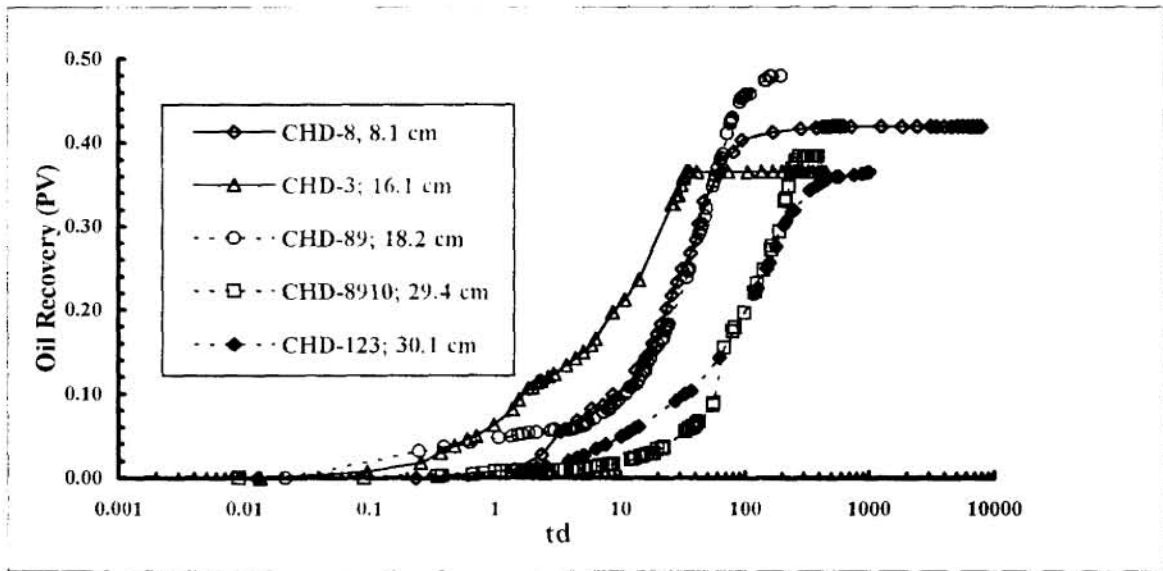


Figure 16. Scaled 1D spontaneous imbibition as function of core length; fractured and unfractured cores.